Gold Nanoparticle Superlattice in Porous Silica and Low Temperature Catalytic CO Oxidation

Shin-Hyun Kang[1]*, Min-Jae Lee[1], Jeeun Lee[1], Jun-Ki Lee[1], Min Gyu Kim[2] and Sung-Min Choi[1]

[1] Department of Nuclear and Quantum Engineering, Korea Advanced Institute of Science and Technology, Daejeon 34141, Republic of Korea, [2] Pohang Accelerator Laboratory, Pohang 37673, Republic of Korea.

*Currently at Chonbuk National University. Correspondence to hunny@kaist.ac.kr

The practical use of nanoparticle superlattices (NPSLs) which are of great interest as materials with designed functionalities[1-5] is often limited by their lack of structural stability under various utilization conditions. Here, we report a new method for directly synthesizing NPSL fully embedded in hierarchically porous silica which provides exceptional stability and efficient pathways for reactant molecules, making the NPSL highly efficient catalyst[6]. The superlattices made of 12 nm gold nanoparticles exhibit exceptionally high catalytic activity for CO oxidation at low temperature, showing higher activity than that of small gold nanoparticles (ca. 3 nm) supported on metal oxides[7]. The gold NPSL also shows unprecedented stability, maintaining its structural stability and catalytic activity without any signature of degradation over a month of continuous catalytic reaction, which present one significant step forward to realizing the great potentials of gold catalysts in automotive emission control and green chemistry industry.

In the most of NPSLs reported so far, the superlattices are formed and maintained by the interactions between the organic ligand molecules grafted on the surface of nanoparticles (NPs). In the drying-mediated method, the ligand-induced inter-particle interactions becomes manifest as the solvent slowly evaporates, inducing the self-assembly of NPs into superlattice in combination with the space filling rules[8-10]. In the DNA-meditated method, the oligonucleotide-grafted NPs self-assemble into a designed superlattice structure due to the programmable nature of DNA[11-14]. The molecular ligand mediated inter-particle interactions or the molecular inter-particle layer, however, can be easily destabilized depending on environmental conditions, making the NPSLs distorted or simply destroyed. For instances, in NPSLs formed by the drying-mediated method, NPs can be easily sintered at high temperature[15], and in the DNA-mediated NPSLs, their morphologies are either distorted or lost entirely when they are removed from the aqueous saline solution or heated above the DNA melting temperature[16]. This lack of structural stability of NPSL often limits their practical applications. Especially, the utilization of NPSLs as catalysts, which is the most important area of application for NPs, has been strongly limited since most of catalytic reaction conditions are very demanding for NPSLs to maintain their structural integrity.

In this study, a new facile method to fabricate highly ordered Au NPSL fully embedded in hierarchically porous silica, which show excellent structural stability at high temperature and unprecedented catalytic activity for CO oxidation at low temperature, has been developed. In this method, monodisperse Au NPs functionalized with thiolated poly(ethylene glycol) (PEG) in water are assembled into highly ordered NPSL through condensation of silica precursors with PEG[17], followed by calcination at high temperature to remove the organic molecules (Fig. 1). The silica matrix provides high structural stability of NPSL and the hierarchically connected meso- and

micro-pores in the superlattice provide efficient pathways for fast access of molecules to the surface of Au NPs, making it highly efficient catalyst[6].

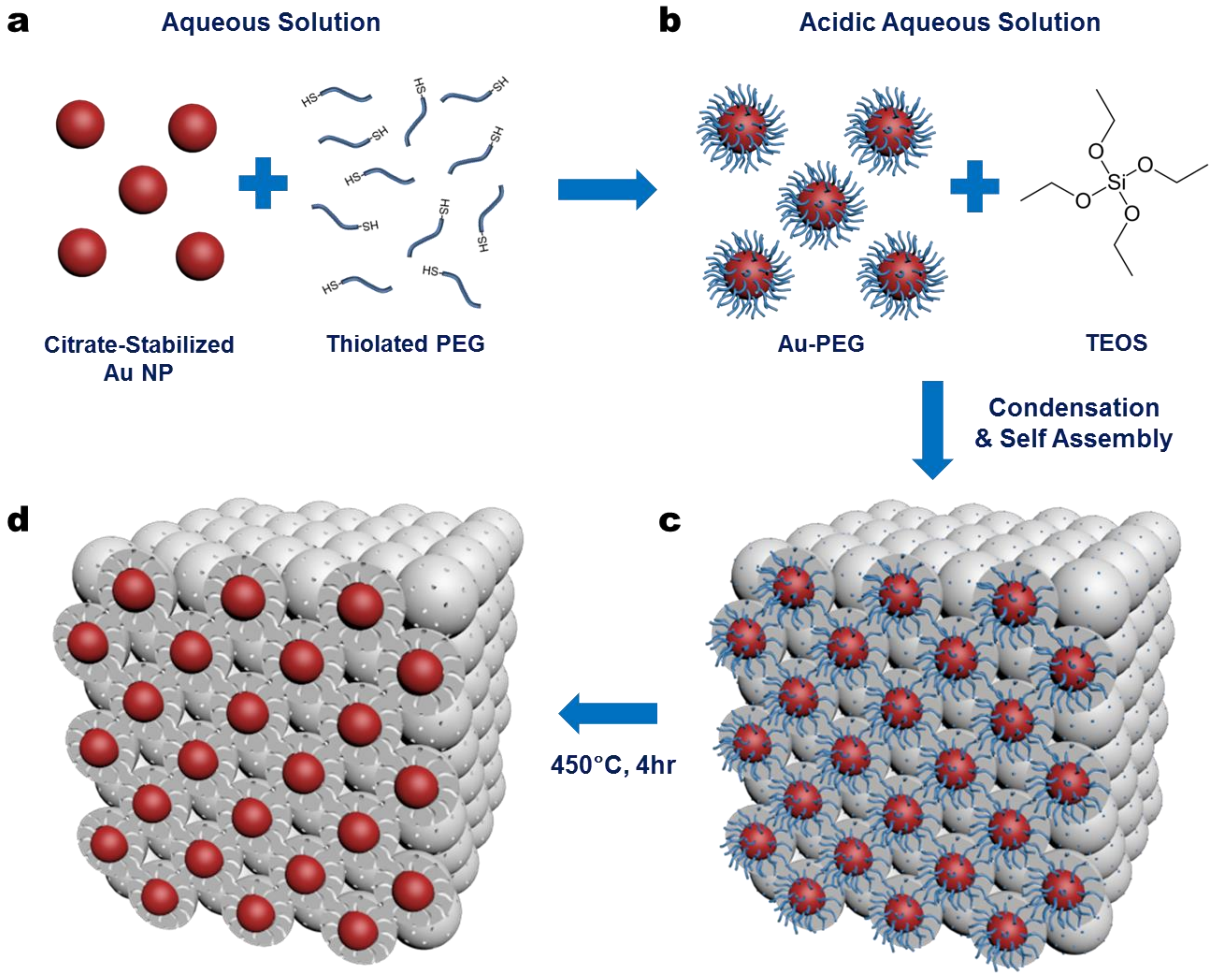

Figure 1. Schematics of synthesis procedure. a, Citrate-stabilized Au NPs are mixed with thiolated PEGs in aqueous solution to form Au-PEG. **b,** TEOS is added into Au-PEG suspension in acidic solution under stirring. **c,** The mixture is left still for 40 hours, resulting in the superlattices by self-assembly. **d,** The superlattices are calcined at 450 °C under helium to pyrolize PEGs in the superlattices.

The superlattice of 12 nm Au NP embedded in porous silica is demonstrated as a model system here. Citrate-stabilized 12 nm Au NPs were synthesized using a previously reported method[18]. The as-synthesized Au NPs were grafted with thiolated PEGs of two different molecular weights (1 and 2 kDa), forming Au-PEG core-shell nanoparticles with two different shell thicknesses (denoted as Au-PEG-1 and -2, respectively). Au-PEGs were homogeneously suspended in acidic aqueous solution, and tetraethyl orthosilicate (TEOS) was mixed with the suspension, producing solid black precipitates (denoted as Au-PEG-Silica-1 and -2). The solid precipitates were washed with water and calcined at 450 ℃ in helium (denoted as Au-Silica-1 and -2). (See Methods for details)

The small angle x-ray scattering (SAXS) intensities of Au-PEG-Silica-1 and -2 (before calcination) show distinct reflections including high order peaks which are well indexed with the face-centered cubic (fcc) symmetry, indicating that highly ordered superlattices with the fcc symmetry are formed in both samples (Fig. 2a). The nearest neighboring inter-particle distances of Au-PEG-Silica-1 and -2 are 19.1 and 21.4 nm, respectively. This shows that the inter-particle distance can be tuned by varying the chain length of thiolated PEG. The SAXS intensities of Au-Silica-1 and -2 (after calcination) also show distinct reflections which are essentially the same as those of the samples before calcination, except a small shift to higher q position (Fig. 2b). This indicates that the morphology of Au NPSLs is fully maintained without any degradation during the calcination at 450 ℃, except a small shrinkage which is typically observed in the synthesis of mesoporous silica. The nearest neighboring inter-particle distances of Au-Silica-1 and -2 are 16.3 and 18.5 nm, respectively.

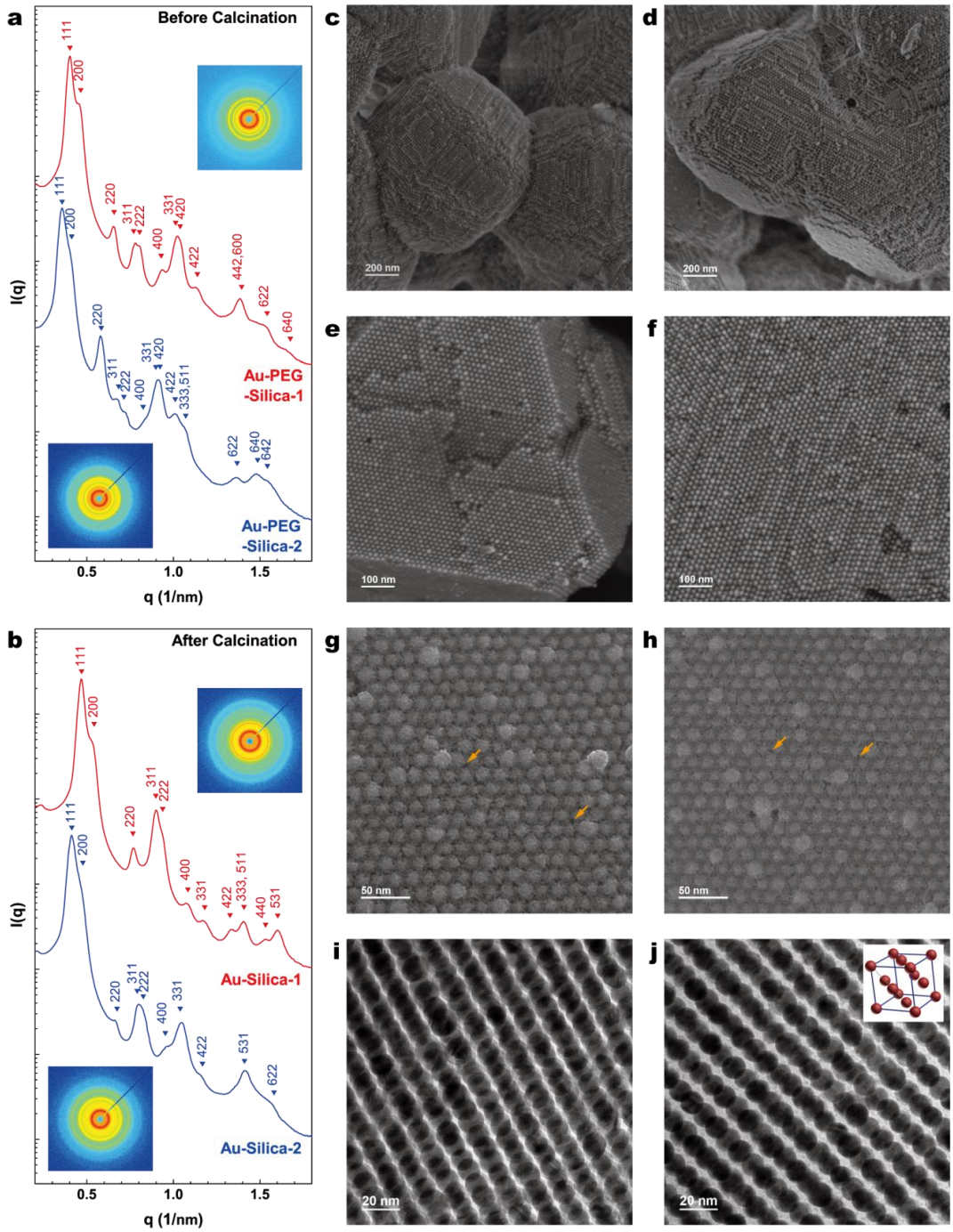

Figure 2. **a, b,** SAXS intensities of Au-PEG-Silica-1 and -2 **(a)**, and Au-Silica-1 and -2 **(b)**. Insets are corresponding 2-D SAXS patterns. **c, d,** SEM images of Au-Silica-1 **(c)** and Au-Silica-2 **(d)**. Backscattered SEM images of Au-Silica-1 **(e)** and Au-Silica-2 **(f)**. **g, h,** SEM images of Au-PEG-Silica-2 (uncalcined) **(g)** and Au-Silica-2 (calcined) **(h)**. **i, j,** TEM images of Au-Silica-1 **(i)** and Au-Silica-2 **(j)** sliced by focused ion beam.

The field emission scanning electron microscopy (FE-SEM) images of Au-Silica-1 and -2 show highly ordered superlattices of Au NPs encapsulated with silica (Fig. 2c – 2f). The (111) and (100) planes, which are the lowest surface energy facets in the fcc crystal[19], are most frequently observed with some steps between the planes in the faceted superlattices of micron size. The distances between the nearest neighboring Au NPs estimated from the images are 16 and 19 nm for Au-Silica-1 and -2, respectively, which are consistent with the SAXS results. The high resolution FE-SEM images of Au-PEG-Silica-2 (before calcination) and Au-Silica-2 (after calcination) show the surface morphologies of the superlattices (Fig. 2g, 2h). It is clear that Au NPs encapsulated with silica shell are packed together and mesopores of a few nm are easily found between silica-encapsulated Au NPs as indicated by arrows. The TEM images of Au-Silica-1 and -2 sliced by the focused ion beam technique show that Au NPs are highly lined up along parallel straight lines, which correspond to the projections along the (111) planes as indicated in the inset (Fig. 2i, 2j). The spacings between the (111) planes estimated from these images are 13 and 15 nm for Au-Silica-1 and -2, respectively, which are consistent with the SAXS and FE-SEM results.

N_2 adsorption and desorption isotherms were measured for Au-Silica-1 and -2 (Fig. 3a, 3b). The pore size distributions evaluated from the adsorption curves by using the density functional theory method[20] show clear bimodal distributions, a narrow distribution peaked at ca. 1 nm (micropores) and a broad distribution ranging from 2 to 10 nm (mesopores) (Fig. 3c, 3d). The porosities of Au-Silica-1 and -2 are 39 and 36 %, respectively. The micropores can be attributed to the pyrolysis of PEG molecules attached to Au NPs during calcination. The mesopores are interstitial voids between closely packed silica-encapsulated Au NPs as indicated by the FE-SEM images. This hierarchical pore structure, in which the mesopores provide highways and micropores provide local roads branched from the highways, respectively, is an important feature to allow fast

access of reactant molecules to the surfaces of Au NPs[6]. The small silica shell thickness (ca. 2-3 nm) is an advantage for the fast access. Inductively coupled plasma mass spectroscopy (ICP-MS) measurements revealed that the contents of Au NPs in Au-Silica-1 and -2 are 78.9 and 73.4 % by weight, respectively. To the best of our knowledge, this is the highest loading of Au NPs in porous silica.

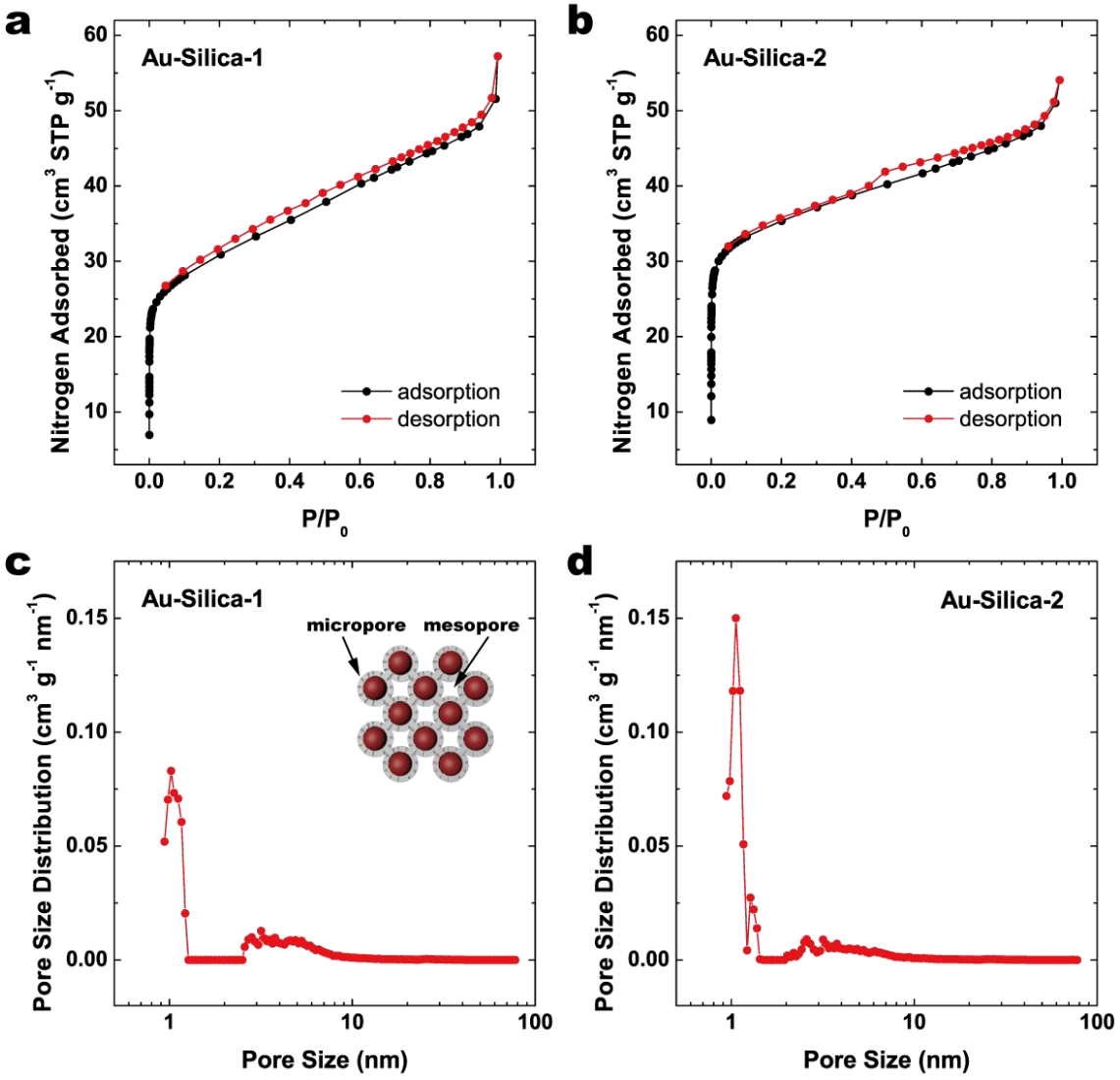

Figure 3. a, b, Nitrogen sorption isotherms of Au-Silica-1 **(a)** and Au-Silica-2 **(b)**. **c, d,** Corresponding pore size distributions of Au-Silica-1 **(c)** and Au-Silica-2 **(d)**. Inset presents the schematic view of micro- and meso-pores.

It has been well reported that Au NP is catalytically very active for CO oxidation at room temperature when small Au NPs (2 - 4 nm) are deposited on reducible metal oxides such as TiO_2. However, Au NPs are not quite active when they are larger than ca. 5 nm or deposited on SiO_2[21]. In contrast to the current knowledge, Au-Silica-1 and -2 which are made of 12 nm Au NPs encapsulated with porous silica (SiO_2) show unprecedented catalytic activity for CO oxidation at room temperature. The catalytic activity of Au-Silica-1 and -2 (100 mg for each) for CO oxidation at room temperature was measured under a total gas flow rate of 100 ml/min and a gas composition of 1 % CO, 10 % O_2 and 89 % He (Fig. 4a). Surprisingly, the superlattices showed 100 % conversion of CO to CO_2. This is the first demonstration of 100 % CO conversion at room temperature with Au NPs as large as 12 nm which is much larger than typical catalytically active Au NPs for CO oxidation. When the temperature was lowered to ca. -50 ℃ (cooled by a dry ice jacket), the superlattices still maintained 100 % CO conversion. The CO conversion rate of Au-Silica-1 at room temperature was stably maintained at 100 % for more than a month of continuous catalytic CO oxidation reaction (Fig. 4b). To the best of our knowledge, the catalytic stability of the superlattice is superior than any other catalyst for CO oxidation reported so far. To confirm that the surprising catalytic activity and stability of Au NPSLs in porous silica are valid with smaller gold particles in the sense of the economic feasibility, a superlattice of 4nm Au particles in porous silica (4-Au-Silica) was fabricated and tested for catalytic CO oxidation. 4-Au-Silica also maintained 100 % of CO conversion for more than a month of catalytic reaction (Figure 4b).

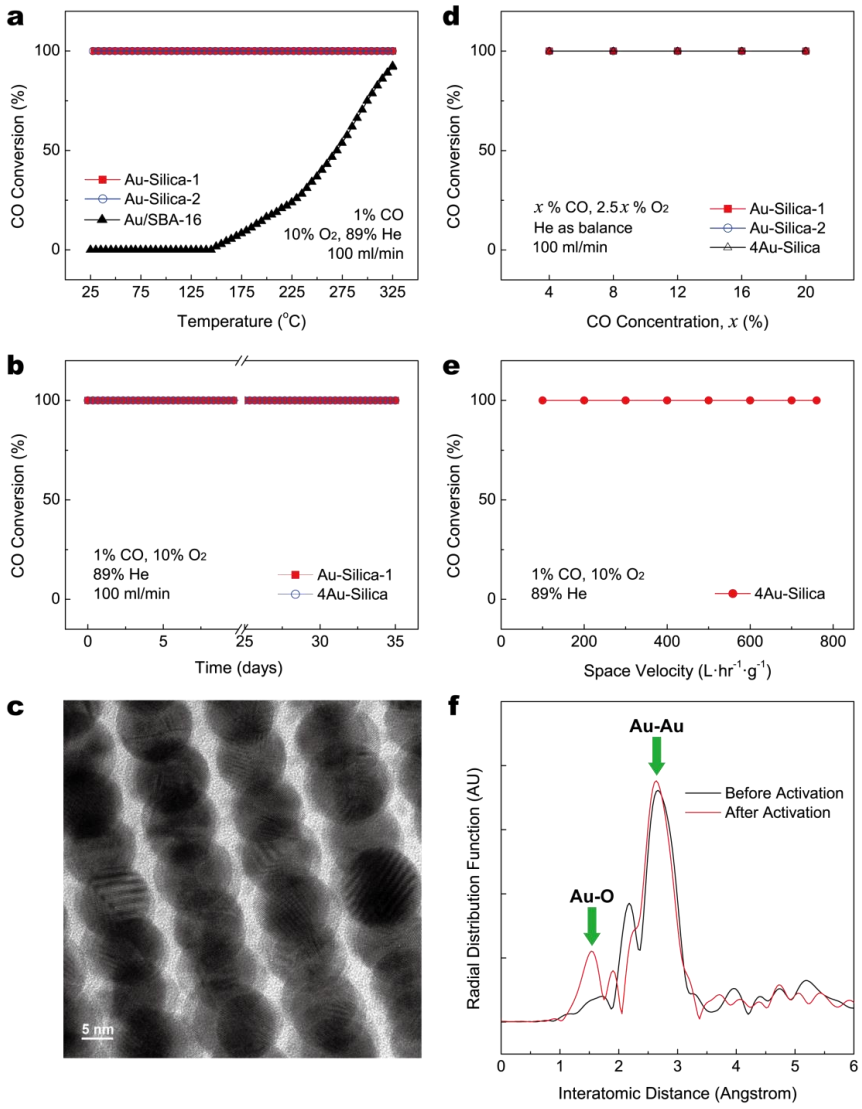

Figure 4. a, CO conversion rate vs. temperature of Au-Silica-1 and -2 (100 mg for each). As a comparison, CO conversion of 12 nm Au NPs sparsely dispersed in SBA-16 mesoporous silica (100 mg) is presented, which shows no conversion of CO below 140 °C. **b,** CO conversion rates at room temperature vs. reaction time for Au-Silica-1 (100 mg) and 4Au-Silica (30 mg). **c,** TEM image of Au-Silica-2 after catalytic reaction for 100 hours including 4 times of high temperature reaction at 325 °C. **d,** CO conversion rate of Au-Silica-1, -2 (60 mg for each) and 4Au-Silica (30mg) at high CO flow rates (excessive exothermic heat was removed by a dry ice jacket). **e,** CO conversion rate of 4Au-Silica (30mg) at high space velocities. **f,** Radial distribution functions of Au-Silica-1 before and after activation that are obtained from the Fourier transform of k^2-weighted Au L_{III}-edge EXAFS signals.

The TEM image of the superlattices, after more than 100 hours of catalytic reaction including 4 times of high temperature reactions at ca. 325 ℃, clearly shows individual Au NPs without any agglomeration or sintering (Fig. 4c). This indicates that all Au NPs in the superlattices are stably protected by porous silica shells, overcoming the particle sintering problem of supported Au NP catalysts under reaction conditions which have been a key hurdle for the industrial use of Au catalysts[22]. The 100% CO conversion was fully maintained even when the CO content was increased by 20 times (20% CO, 50% O_2 and 30% He, 100 ml/min, Fig. 4d). During these measurements, the temperature was kept below 25 ℃ by removing exothermic heat generated by the massive CO oxidation with a dry ice jacket. This is in stark contrast to the current understanding of the particle size and support material effects in heterogeneous gold nanoparticle catalysts for CO oxidation at low temperature[23,24]. To see how compact and how efficient a catalyst system can be made of the Au NPSLs in porous silica, the space velocity was increased up to 760,000 mL (1% CO, 10% O_2 and 89% He) per hour per gram of catalyst for 4-Au-Silica, and the 100 % CO conversion rate was maintained within the whole range of space velocity. This value of space velocity with 100% of conversion rate has never been reached by gold catalysts to the best of our knowledge.

To investigate the origin of high catalytic activity of the Au NPSLs in porous silica, extended x-ray absorption fine structure (EXAFS) measurements were performed for the superlattices before and after activation for CO oxidation (See Methods). The radial distribution functions obtained from the EXAFS data show that Au-O component is clearly present in the activated Au NPSLs while it is not observed in the Au NPSLs before activation[27] (Fig. 4f and Fig. S15). Since the EXAFS measurements were performed after one month after the activation, the results clearly indicate that fairly stable Au-O chemical bonds are formed. This is very unusual for Au NPs since

Au-O complex is well known to be spontaneously reduced due to the endothermic chemisorption energy of oxygen on gold[28]. The close proximity between the surface of Au NPs and tightly encapsulating porous silica may provide a condition to form stable Au-O bonds at the interface between Au NP and encapsulating mesoporous silica, possibly in the form of Au-O-Si, resulting in a surface-modified Au NP. Since Au-oxide is a reducible metal-oxide, it is tempting to consider a possibility that the stable Au-O complexes on Au NPs in the superlattices play the role of a reducible metal-oxide support which is the key element for high catalytic activity of heterogeneous Au catalysts for CO oxidation[24]. Therefore, the unique configuration of the superlattices, in which all the surfaces of Au NPs containing Au-O complexes are accessible by CO and O_2 molecules through hierarchical porous pathways, may contribute to the high catalytic activity. This is in contrast with the typical supported Au NP catalysts in which the perimeter zone of Au NPs surrounded by reducible metal oxide surface sites are considered as active zone for CO oxidation[29,30]. To understand the role of the Au-O complexes in the Au NPSL confined in porous silica for CO oxidation as well as their formation and stability, however, further investigations are required.

While the full CO oxidation mechanism in the superlattices remains to be understood, the synthesis method developed in this study provides a new route for designing highly active and stable heterogeneous Au catalysts. Furthermore, the synthesis method can be applicable for other inorganic NPSLs and extended for multi-component NPSLs, providing new opportunities for fabricating ultra-stable metamaterials with tailored properties and their practical applications.

Methods

Preparation of PEG-functionalized Au NPs. Citrate-stabilized gold nanoparticles were synthesized by the method of ref. 18. 500 mL of 1 mM $HAuCl_4 \cdot 3H_2O$ aqueous solution was brought to a rolling boil with vigorous stirring in a 1L round flask equipped with a condenser. 50 mL of 38.8 mM trisodium citrate aqueous solution was rapidly added to the flask, which induced an immediate change of color from yellow to burgundy red. Boiling of the solution was continued for 10 minutes and stirring was continued for additional 15 minutes after removal of heating. The as-synthesized Au NPs were functionalized with SH-PEGs of different molecular weights, 1 and 2 kDa. For this, 1 g of SH-PEG was added into 2.2 L of as-prepared colloidal Au NP solution and the mixture was shaken overnight with aluminum foil wrapping. The unbound polymers were removed by 3 times of successive centrifuges (at 75,000 g for 1 hour for each). The centrifuged Au NPs were freeze-dried and re-dispersed in water at concentrations as needed.

Synthesis of Au NP superlattice. To synthesize the Au NPSL embedded in porous silica, Au-PEG (0.21 g and 0.17 g for Au-PEG-1 and -2, respectively) was homogeneously suspended in 1 ml of 1.6 M HCl aqueous solution, and 0.17 g of TEOS was added into the suspension. The mixture was stirred for 15 minutes and then left at room temperature for 40 hours without stirring. The solid black precipitates (Au-PEG-Silica-1 and -2) were washed with water and dried, followed by calcination at 450 ℃ under helium to remove PEG molecules.

Structural analyses. SAXS and EXAFS measurements were carried out using the 4C and 10C beamlines at the Pohang Light Source (PLS-II), respectively. Field emission scanning electron microscopy (FE-SEM) measurements were performed using Magellan 400 (FEI) at KAIST Analysis Center for Research Advancement and S-5500 (Hitachi) at KBSI Jeonju Center. TEM measurements were performed using a 300 kV FE-TEM (Tecnai G2 F30, FEI), and the samples were sliced using the focused ion beam (Quanta 3D FEG, FEI at KBSI) technique to measure the internal region of the superlattices. N_2 adsorption and desorption measurements of the Au NPSLs were performed using Autosorb-iQ (Quantachrome).

Measurement of catalytic activity. Catalytic oxidation of CO with Au NPSLs was performed in a flow reactor which was connected to mass flow controllers (Line Tech) and a gas chromatography (DS Science). The sample (Au-Silica-1 or -2) was loaded in a cylindrical quartz

tube filled with quartz wool in the middle. Subsequently, the loaded sample was heated to 350 ℃ (under a total gas flow rate of 100 ml/min and a gas composition of 1% CO, 10% O_2 and 89% He) and cooled down to room temperature. All the CO oxidation measurements were performed after this activation treatment.

References

1. Nie, Z., Petukhova, A. & Kumacheva, E. Properties and emerging applications of self-assembled structures made from inorganic nanoparticles. *Nature Nanotechnol*. **5**, 15-25 (2010).
2. Ross, M. B., Ku, J. C., Vaccarezza, V. M., Schatz, G. C. & Mirkin, C. A. Nanoscale form dictates mesoscale function in plasmonic DNA–nanoparticle superlattices. *Nature Nanotechnol*. **10**, 453-458 (2015).
3. Kagan, C. R. & Murray, C. B. Charge transport in strongly coupled quantum dot solids. *Nature Nanotechnol.* **10,** 1013–1026 (2015).
4. Kasyutich, O., Desautels, R. D., Southern, B. W. & van Lierop, J. Novel aspects of magnetic interactions in a macroscopic 3D nanoparticle-based crystal. *Phys. Rev. Lett.* **104**, 127205 (2010).
5. Li, J. *et al.* Nanoparticle superlattices as efficient bifunctional electrocatalyst for water splitting. *J. Am. Chem. Soc.* **137**, 14305-14312 (2015).
6. Pérez-Ramírez, J., Christensen, C. H., Egeblad, K., Christensen, C. H. & Groen, J. C. Hierarchical zeolites: enhanced utilisation of microporous crystals in catalysis by advances in materials design. *Chem. Soc. Rev.* **37**, 2530-2542 (2008).
7. Haruta, M. Nanoparticulate gold catalysts for low-temperature CO oxidation. *J. New Mater. Electrochem. Syst.* **7**, 163–172 (2004).
8. Shevchenko, E. V., Talapin, D. V., Kotov, N. A., O'Brien, S. & Murray, C. B. Structural diversity in binary nanoparticle superlattices. *Nature* **439**, 55–59 (2006).
9. Paik, T., Diroll, B. T., Kagan, C. R. & Murray, C. B. Binary and ternary superlattices self-assembled from colloidal nanodisks and nanorods. *J. Am. Chem. Soc.* **137,** 6662–6669 (2015).
10. Henzie, J., Grünwald, M., Widmer-Cooper, A., Geissler, P. L. & Yang, P., Self-assembly of uniform polyhedral silver nanocrystals into densest packings and exotic superlattices. *Nature Mater.* **11**, 131-137 (2011).

11. Park, S. Y., Lytton-Jean, A. K. R., Lee, B., Weigand, S., Schatz, G. C. & Mirkin, C. A. DNA-programmable nanoparticle crystallization. *Nature* **451**, 553-556 (2008).
12. Nykypanchuk, D., Maye, M. M., van der Lelie, D. & Gang, O. DNA-guided crystallization of colloidal nanoparticles. *Nature* **451**, 549-552 (2008).
13. Jones, M. R., Seeman, N. C. & Mirkin, C. A. Programmable materials and the nature of the DNA bond. *Science* **347**, 1260901 (2015).
14. Zhang, Y. *et al.* Selective transformations between nanoparticle superlattices via the reprogramming of DNA-mediated interactions. *Nature Mater.* **14**, 840-847 (2015).
15. Kang, Y. *et al.* Engineering catalytic contacts and thermal stability: gold/iron oxide binary nanocrystal superlattices for CO oxidation. *J. Am. Chem. Soc.* **135**, 1499-1505 (2013).
16. Auyeung, E., Macfarlane, R. J., Choi, C. H. J., Cutler, J. I. & Mirkin, C. A. Transitioning DNA-engineered nanoparticle superlattices from solution to the solid state. *Adv. Mater.* **24**, 5181-5186 (2012).
17. Zhao, D., Huo, Q., Feng, J., Chmelka, B. F. & Stucky, G. D. Nonionic triblock and star diblock copolymer and oligomeric surfactant syntheses of highly ordered, hydrothermally stable, mesoporous silica structures. *J. Am. Chem. Soc.* **120**, 6024-6036 (1998).
18. Grabar, K. C., Freeman, R. G., Hommer, M. B. & Natan, M. J. Preparation and characterization of Au colloid monolayers. *Anal. Chem.* **67**, 735-743 (1995).
19. Wulff, G. On the question of speed of growth and dissolution of crystal surfaces. *Z. Krystallogr. Mineral.* **34**, 449–530 (1901).
20. Landers, J., Gor, G. Y. & Neimark, A. V. Density functional theory methods for characterization of porous materials. *Colloids Surf. A* **437**, 3-32 (2013).
21. Janssens, T. V. W. *et al.* Insights into the reactivity of supported Au nanoparticles: combining theory and experiments. *Top. Catal.* **44**, 15-26 (2007).
22. Han, C. W. *et al*. Highly stable bimetallic AuIr/TiO2 catalyst: physical origins of the intrinsic high stability against sintering. *Nano Lett*. **15**, 8141-8147 (2015).
23. Lopez, N. *et al.* On the origin of the catalytic activity of gold nanoparticles for low-temperature CO oxidation. *J. Catal.* **223,** 232–235 (2004).
24. Liu, X. Y., Wang, A., Zhang, T. & Mou, C.-Y. Catalysis by gold: new insights into the support effect. *Nano Today* **8**, 403-416 (2013).

25. Chen, M. S., Goodman, D. W. The structure of catalytically active gold on titania. *Science* **306**, 252-255 (2004).
26. Haruta, M. Chance and necessity: my encounter with gold catalysts. *Angew. Chem. Int. Ed.* **53**, 52-56 (2014).
27. Yang, J. H. *et al.* Activation of Au/TiO2 catalyst for CO oxidation. *J. Phys. Chem. B* **109**, 10319-10326 (2005).
28. Ono, L. K. & Cuenya, B. R. Formation and thermal stability of Au_2O_3 on gold nanoparticles: size and support effect. *J. Phys. Chem. C* **112**, 4676-4686 (2008).
29. Green, I. X., Tang, W., Neurock, M. & Yates Jr., J. T. Spectroscopic observation of dual catalytic sites during oxidation of CO on a Au/TiO2 catalyst, *Science* **333**, 736-739 (2011).
30. Widmann, D. & Behm, R. J. Activation of molecular oxygen and the nature of the active oxygen species for CO oxidation on oxide supported Au catalysts. *Acc. Chem. Res.* **47**, 740-749 (2014).

Acknowledgments

We thank Prof. H. C. No at KAIST for providing a gas chromatography instrument, C.-H. Jung and Prof. J.Y. Park at KAIST for their help in an initial test for CO oxidation and valuable discussion. We also thank the Pohang Light Source and the HANARO Neutron Research Center for providing access to the beamlines used in this work. This work was financially supported by the NRF grants funded by the MEST of the Korean government (No. 2014R1A2A1A05007109 and 2011-0031931), KAERI grant and KUSTAR-KAIST Program grant.

Author Contributions

S.H.K. designed the experiments. S.M.C. supervised the experiments. S.H.K., M.J.L., J.L. and J.K.L. contributed to the synthesis of gold nanoparticle superlattices. S.H.K. performed CO oxidation experiments. M.G.K. conducted EXAFS experiments. S.H.K. and S.M.C. co-wrote the paper. All authors discussed the results and commented on the manuscript.